hydrogen

MDPI

Article

Hybrid Renewable Hydrogen Energy Solution for Remote Cold-Climate Open-Pit Mines

Hosein Kalantari * and Seyed Ali Ghoreishi-Madiseh

NBK Institute of Mining Engineering, University of British Columbia, Vancouver, BC V6T 1Z4, Canada
* Correspondence: hoseink@mail.ubc.ca

Abstract: Contemporary off-grid mining operations rely on diesel fuel for the provision of their total energy including electricity, heat, and haulage. Given the high cost of diesel and its imposed greenhouse gas emissions, mining companies are looking for more affordable and cleaner sources of energy for their operations. Although renewable energy systems, such as solar photovoltaic and wind provide efficient solutions to address this challenge, full decarbonization has shown to be very challenging, mainly due to the high cost of battery storage along with the inability to meet total site energy demand. Integrating hydrogen and thermal storage with battery banks can facilitate a full transitioning off diesel. In this sense, the present study intends to offer an innovative decarbonized solution by integrating wind turbines with a multi-storage system (battery, hydrogen, and thermal storage) to supply the total energy (electricity, heat, and haulage) for remote open-pit mines. Among the different proposed fully decarbonized configurations in this study, it is shown that a renewable system with a hydrogen-powered fleet and hybridized battery/hydrogen storage configuration can present the most economically viable case for open-pit mines with a considerably less life-of-mine cost.

Keywords: renewable energy; open-pit mine; decarbonization; hydrogen; thermal storage; remote mines; wind

Citation: Kalantari, H.; Ghoreishi-Madiseh, S.A. Hybrid Renewable Hydrogen Energy Solution for Remote Cold-Climate Open-Pit Mines. *Hydrogen* **2022**, *3*, 312–332. https://doi.org/10.3390/hydrogen3030019

Academic Editor: Sergey Verevkin

Received: 13 July 2022
Accepted: 9 August 2022
Published: 12 August 2022

1. Introduction

Mining operations are complex industrial systems comprised of a diverse set of activities seeking the extraction of minerals. These activities (such as blasting, drilling, comminution, excavation, tailing storage and material handling) are mostly interdependent and need specific types of techniques and machinery. Moreover, most mining operations are extremely energy intensive and expensive to maintain. In fact, a fully developed off-grid mine usually requires millions of liters of diesel per annum to operate [1]. Burning such large quantities of diesel is not only very costly, but also environmentally harmful. This makes mining one of the main contributors to global GHG (greenhouse gases) and carbon emissions. At this time, mining is responsible for 4–7% of global GHG emissions and 2–3% of global carbon emissions [2]. To overcome this energy–economic–environmental challenge, miners all over the world are now looking for opportunities to employ fully decarbonized energy solutions.

Although some efforts have been directed towards the decarbonization of mine sites over the last decade, a net zero mining operation is still a work in progress. Among the Canadian examples, is the Diavik Diamond mine in the Northwest Territories, Canada, which has employed a 9.2 MW wind farm composed of quadruple 2.3 MW turbines since 2012 to meet ten percent of the site's electricity demand. According to the mine's annual reports, 3.8 million liters of diesel were displaced by the installed renewable power plant in 2013. The capital cost of the project was CAD 31 million, and it is expected to breakeven in eight years [3]. Following in the Diavik Diamond mine's footsteps, is another mining operation in Canada, the Raglan nickel mine located in Quebec, which has been implementing a wind farm with a total capacity of 6 MW integrated with a

multi-storage system with the capacity of 3 MW since 2015 to meet ten percent of the site's total energy demand. The renewable power plant adds the benefit of reducing the site's diesel consumption and GHGs by displacing 4.4 million liters of diesel and cutting down 12,000 tonnes of carbon emissions [4]. Although there are a few cases of successful renewable energy adoption in Canadian mining operations, they have not contributed more than 20% of a site's electric load (5% to 10% of the total energy loads) [5]. The high cost of battery storage solutions [6,7] coupled with an inability to meet total site energy demands are the primary limiting factors to the full decarbonization of a mine's power system. Hybridizing battery banks coupled with relatively less expensive storage systems such as hydrogen and rock-pile thermal storage can help with mitigating the remarkable financial burden of energy storage and accelerate the transition rate from diesel to renewable mine energy systems.

There are several studies reported in the literature investigating hydrogen and thermal storages for application in smaller-scale decarbonized energy systems, and some of them are summarized in Table 1.

Table 1. Studies of storage systems for application in smaller-scale decarbonized energy systems.

Storage Type	Application	Summary	Reference
Hydrogen storage	Wind/solar renewable energy system	Their results confirm the positive impact of hydrogen and fuel cells for storage and transportation applications.	Uyar et al. [8]
Hydrogen storage	Hybrid solar/wind energy system	The results of their tests showed a fair exergy efficiency for electrolyzer (68.75%) and quite low for fuel cell (35.9%). The lowest efficiency is reported to be the PV modules (8.39%).	Calderon et al. [9]
Hydrogen storage	Hybrid solar/wind energy system for a residential application in Bozcaada Island, Turkey	The energy and exergy efficiency of PV array were found to be 13.31% and 14.26%, respectively. Similarly, these efficiencies for wind turbine and electrolyzer were, respectively, reported to be 46%, 50.12%, 59.68% and 60.26%.	Kalinci et al. [10]
Multi-storage (battery-hydrogen)	Hybrid solar/wind energy system for a residential application in the Lake Baikal coast	According to the results of their study, integrating hydrogen storage to the system substantially improves the economic performance of the system.	Marchenko et al. [11]
Hydrogen storage	Solar renewable energy system for application in Kirklareli university campus in Turkey	The optimal scenario was reported to be the grid-connected PV hybrid system with USD0.256/kWh levelized cost of electricity.	Dursun [12]
Hydrogen storage	Hybrid solar/wind energy system for residential application in Oshawa, Canada	The exergy and energy efficiencies of the proposed renewable system are calculated to be 26.8% and 26%, respectively. Additionally, the levelized cost of electricity supplied by the renewable system was reported to be USD0.862/kWh.	Khalid et al. [13]
Borehole thermal storage	Solar renewable energy system for residential applications in Anneberg, Sweden	Despite low efficiencies of some of the studies scenarios, the idea was found to be feasible for the case study.	Lundh and Dalenbäck [14]
Rock-pile seasonal thermal storage	Waste thermal energy from diesel generator exhaust in arctic regions	The thermal storage system was revealed to be feasible for the investigated case study with less than 5 years of payback period.	Amiri et. al. [15]
Multi-storage (battery -hydrogen-thermal storage)	Wind renewable energy system for application in underground mines	According to the results of the study, renewable system with battery electric vehicles and multi-storage (battery-hydrogen-thermal storage) configuration was revealed to be the most favorable scenario for application in underground mines.	Kalantari et al. [16]

With the increasing demand and growth in renewable solutions among miners, some mining companies are conceiving an all-renewable-based mine total energy system. To the best of the authors' knowledge, no study has yet been conducted targeting the full

decarbonization of open-pit mining operations in cold climates. Accordingly, this research work aims to propose a stand-alone net zero energy system for open-pit mining operations in arctic remote sites by hybridizing renewable wind generation and multi-storage energy solutions to supply the mine total energy demands including electricity, motive, and heat. This study intends to evaluate the possibility of employing the proposed all-renewable system for different locations, by presenting sensitivity analyses of the wind speed and energy market prices.

2. Methodology and Assumptions

Two types of surface mining with minimal and intensive comminution and mineral processing (C&MP) are addressed in the present research study. To obtain cost estimations from the simulations, an energy profile of the mining operation is needed. In this sense, the total energy demands (including electricity, heat, and motive) of each case were established based on the data acquired from Natural Resources Canada [17]. The energy profile of each case is shown in Figure 1. For every kiloton of extracted ore in a typical open-pit mining operation with minimal C&MP, the mine needs 20.7 MWh of which 48% is for electricity, 42% is for mobile equipment, and 10% is for heat demand. On the other hand, a typical open-pit mine with intensive C&MP requires 35.5 MWh for every kiloton of ore, of which 66% of that is for electricity, 28% is for mobile equipment, and 6% is for heat demands.

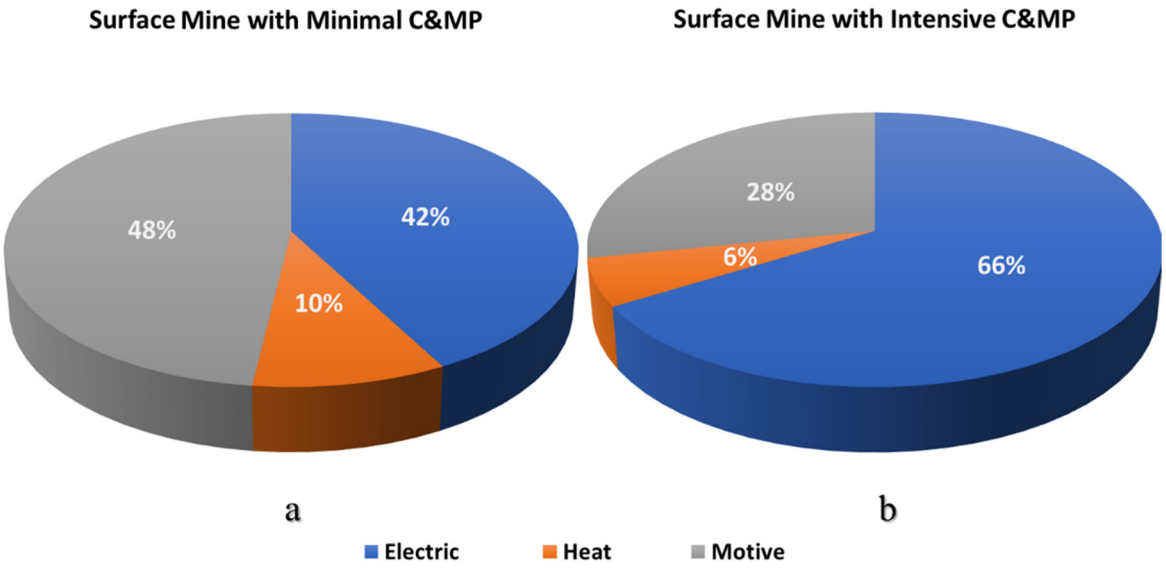

Figure 1. Energy profile of a typical open-pit mining operations: (**a**) Open-pit mine with minimal C&MP; (**b**) open-pit mine with intensive C&MP [17].

The conventional all-diesel system and the proposed fully decarbonized alternative scenarios are designed in a modular based approach and compared to find the optimum system for each mining case. The modular size is selected to be 5 MW of the site's total energy demand. This means that any of the proposed all-renewable systems can replace the conventional all-diesel system with the total energy size of 5 MW. Modular sizing of the scenarios allows mining companies to operate a mine with a flexible combination of the modules resulting in partially or fully decarbonized systems. The total number of modules to operate a mine can be calculated by:

$$N_{modules} = \frac{P_{tot}}{P_{module}} \quad (1)$$

Here, P_{tot} is the total power demand of the site (including electricity, motive and heat) and P_{module} is the module size (5 MW).

2.1. Conventional All-Diesel System

Figure 2 shows the system configuration for an all-diesel-based energy system. As it can be inferred from this figure, diesel generators (*DG*) are used for electric power supply, diesel-powered fleet (*DPF*) are used for mobile equipment, and diesel boilers (*DB*) are used to meet the heat demands of a site. The diesel consumption per unit of time (liter/s) and its associated costs to meet each of a site's energy component (i.e., electricity (*E*), motive (*M*), and heat (*H*)) can be calculated by [18]:

$$Q_{D,E}(t) = \frac{P_E(t)}{HV_D \cdot \rho_D \cdot \eta_{DG}} \tag{2}$$

$$C_{D,E}(t) = Q_{D,E}(t) \cdot Pri_D \tag{3}$$

$$Q_{D,M}(t) = \frac{P_M(t)}{HV_D \cdot \rho_D \cdot \eta_{DPF}} \tag{4}$$

$$C_{D,M}(t) = Q_{D,M}(t) \cdot Pri_D \tag{5}$$

$$Q_{D,H}(t) = \frac{P_H(t)}{HV_D \cdot \rho_D \cdot \eta_{DB}} \tag{6}$$

$$C_{D,H}(t) = Q_{D,H}(t) \cdot Pri_D \tag{7}$$

Here, P_E, P_M and P_H are the electric, motive and heating power demands of the site. HV_D, Pri_D and ρ_D are the heat value, density, and price of diesel. In addition, η_{DPF}, η_{DG}, and η_{DB} are the diesel fleet, diesel generator and diesel boiler efficiencies, respectively. In order to avoid electric power interruptions, for every three diesel generators, two backup generators are incorporated in the design.

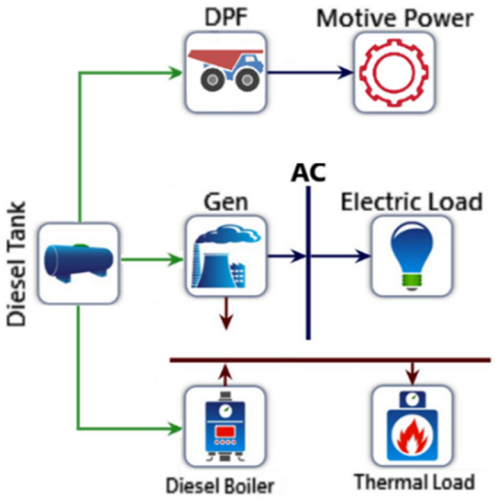

Figure 2. All-diesel-based system configuration.

Greenhouse Gases Emissions

Employing an all-diesel based system is not only very costly for a mine, but also causes severe environmental damages. The intensity of emissions for any pollutant *p* caused by diesel equipment can be expressed by [18]:

$$EM_p(t) = \frac{Q_{D,i}(t)}{EF_p} \tag{8}$$

Here, $Q_{D,i}$ represents the liter of diesel burned in equipment i (DPF, DG, or DB), and EF_p denotes the pollutant p emission factor. One can obtain the net carbon equivalent of emissions and associated costs by:

$$EM_{net,CE}(t) = \sum(EM_p(t) \times \mathrm{GWP_p}) \quad (9)$$

$$Cost_{em}(t) = EM_{net,CE}(t) \times \mathrm{Pen_{CE}} \quad (10)$$

In Equations (9) and (10), Pen_{CE} denotes the carbon penalty imposed by the government, and GWP_p represents the pollutant p global warming potential [19].

2.2. All-Renewable System

The following configurations are considered for alternative renewable systems. Six different all-renewable designs are evaluated in this study with the listed assumptions as follows:

a. All-renewable system with hydrogen-powered fleet (*HPF*) and battery/fc storage configuration (Figure 3):
   - Renewable wind generation/Battery/FC system for electrical load
   - Hydrogen-powered fleet for haulage equipment
   - Electric heater/Thermal storage for thermal load

b. All-renewable system with hydrogen-powered fleet (HPF) and battery storage configuration (Figure 4):
   - Renewable wind generation/Battery system for electrical load
   - Hydrogen-powered fleet for haulage equipment
   - Electric heater/Thermal storage for thermal load

c. All-renewable system with hydrogen-powered fleet (HPF) and fc storage configuration (Figure 5):
   - Renewable wind generation/FC system for electrical load
   - Hydrogen-powered fleet for haulage equipment
   - Electric heater/Thermal storage for thermal load

d. All-renewable system with battery electric fleet (BEF) and battery/fc storage configuration (Figure 6):
   - Renewable wind generation/Battery/FC system for electrical load
   - Battery electric fleet for haulage equipment
   - Electric heater/Thermal storage for thermal load

e. All-renewable system with battery electric fleet (BEF) and battery storage configuration (Figure 7):
   - Renewable wind generation/Battery system for electrical load
   - Battery electric fleet for haulage equipment
   - Electric heater/Thermal storage for thermal load

f. All-renewable system with battery electric fleet (BEF) and fc storage configuration (Figure 8):
   - Renewable wind generation/FC system for electrical load
   - Battery electric fleet for haulage equipment
   - Electric heater/Thermal storage for thermal load

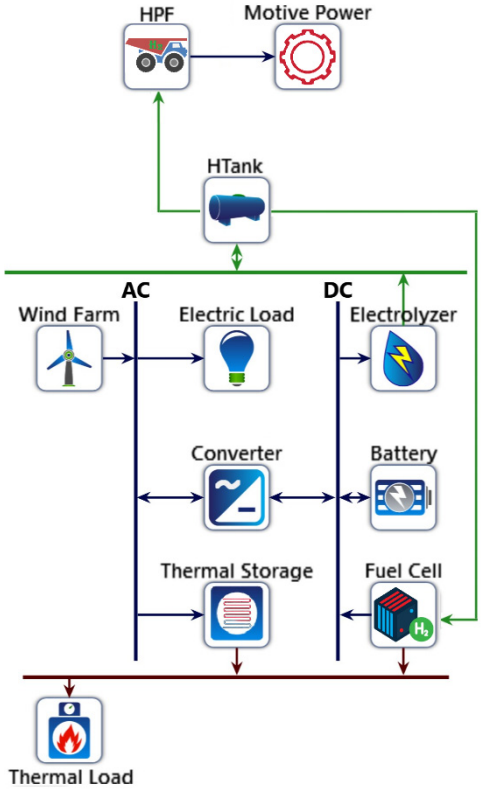

Figure 3. All-renewable system with hydrogen-powered fleet (HPF) and battery/fc (fuel cell) storage configuration.

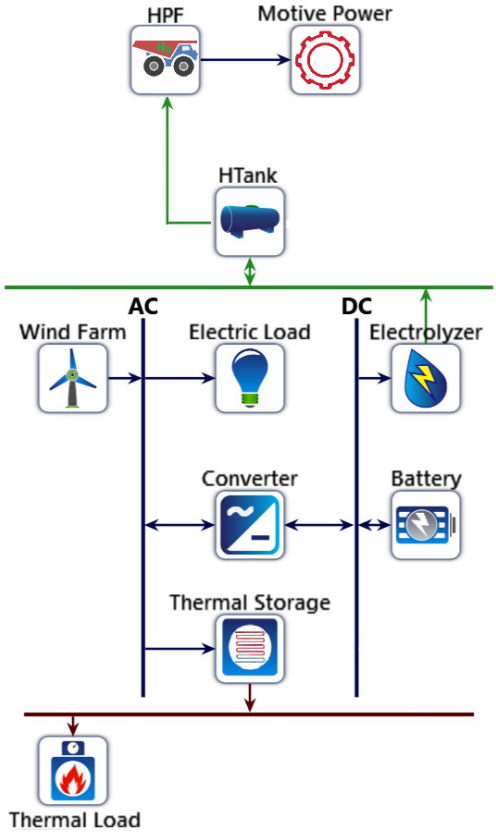

Figure 4. All-renewable system with hydrogen-powered fleet (HPF) and battery storage configuration.

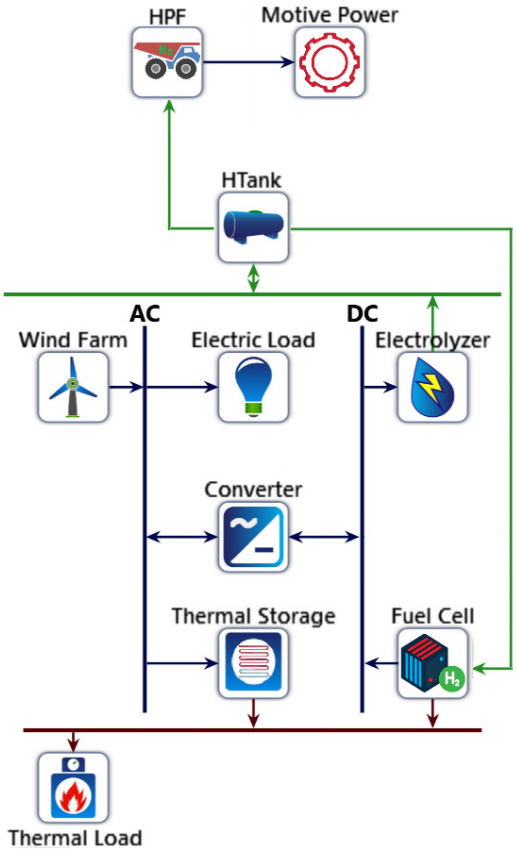

Figure 5. All-renewable system with hydrogen-powered fleet (HPF) and fc storage configuration.

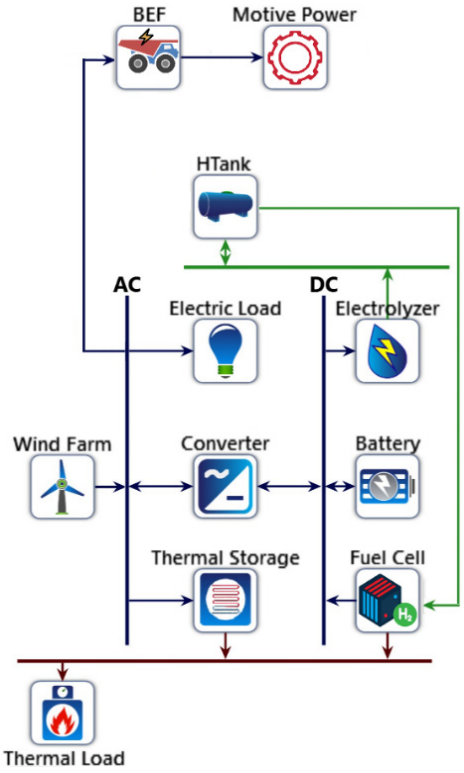

Figure 6. All-renewable system with battery electric fleet (BEF) and battery/fc storage configuration.

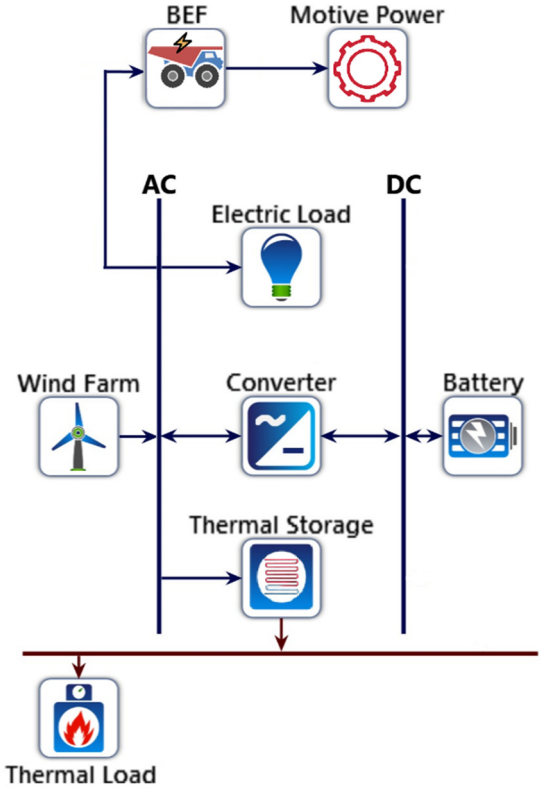

Figure 7. All-renewable system with battery electric fleet (BEF) and battery storage configuration.

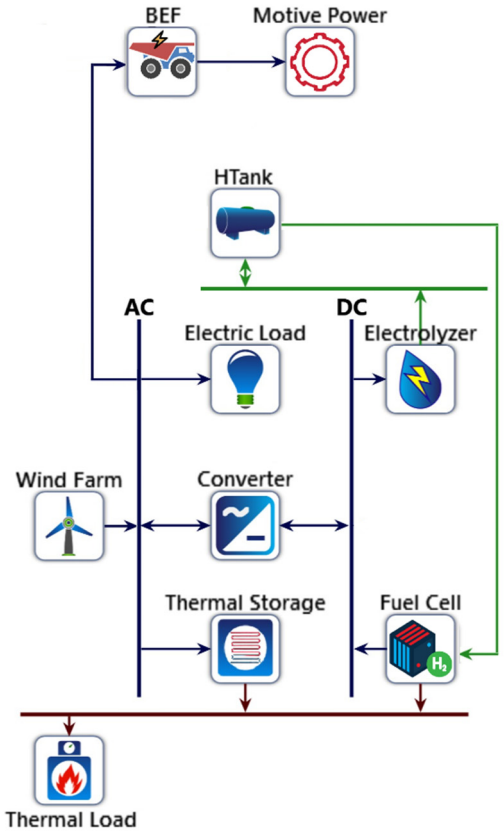

Figure 8. All-renewable system with battery electric fleet (BEF) and fc storage configuration.

Descriptions and numerical modeling of the equipment used in the proposed configurations can be found as follows.

2.2.1. Wind Farm

For all the proposed renewable configurations, wind is considered as the main source of power generation as it has a high potential for the selected case study (a surface mining operation in Canada). One can obtain the wind speed at the height of the turbine hub:

$$V_{hub} = V_{anem}\frac{\ln(z_{hub}/z_0)}{\ln(z_{anem}/z_0)} \tag{11}$$

Here, V_{anem} and z_0 represent the anemometer wind speed and length of the surface roughness, respectively. Additionally, z_{hub} and z_{anem} denote the heights of turbine hub and anemometer, respectively [20].

Using the calculated wind speed at the turbine hub, by fitting it to the power curve, one can obtain the generated power by the wind farm at a standard air density for each time step. For any type of wind turbine, there exists a power curve which the manufacturer provides. One can obtain the power curve by the curve fitting technique [21,22]:

$$P_w(t) = \begin{cases} 0 & if\ V(t) < V_c \\ a_1V^n(t) + \ldots + b_1^2V^2(t) + c_1V(t) + d_1 & if\ V_c \le V(t) < V_1 \\ a_2V^n(t) + \ldots + b_2^2V^2(t) + c_2V(t) + d_2 & if\ V_1 \le V(t) < V_2 \\ a_3V^n(t) + \ldots + b_3^2V^2(t) + c_3V(t) + d_3 & if\ V_2 \le V(t) < V_f \\ a_4V^n(t) + \ldots + b_4^2V^2(t) + c_4V(t) + d_4 & if\ V(t) > V_f \end{cases} \tag{12}$$

In Equation (12), V_c and V_f indicate the cut-in and cut-off speeds, respectively. In order to maximize the curve fitting precision, V_1 and V_2 are used as the intermediate values. The actual power can be determined by:

$$P_{w,ac}(t) = \left(\frac{\rho}{\rho_0}\right)P_w(t) \tag{13}$$

In this equation, ρ and ρ_0 represent the actual and standard condition air density.

2.2.2. Storage Units

The intermittency of renewable energy sources such as solar and wind generation is a challenge in the implementation of such systems that can be addressed by storage units. As the main power source, the generated power from a wind farm supplies a site's energy demand. During a high wind period when the generated power exceeds the demand, it is stored in storage units. On the other hand, during a low wind period when the generated power is not high enough to meet a site's energy demands, a storage unit compensates for the power shortage. Three different types of storage units are incorporated in the proposed configurations, namely, a battery bank, hydrogen storage, and thermal storage.

a. Battery bank:

The charge of a battery bank during the charging and discharge states can be calculated as follows, respectively [21,22]:

$$Charging: \quad C_B(t) = C_B(t-1)(1-\sigma) + \left(P_{w,ac}(t) - \frac{P_L(t)}{\eta_{conv}}\right)\eta_{Batt} \tag{14}$$

$$Discharge: \quad C_B(t) = C_B(t-1)(1-\sigma) + \left(\frac{P_L(t)}{\eta_{conv}} - P_{w,ac}(t)\right) \tag{15}$$

In Equations (14) and (15), η_{Batt}, σ and η_{Conv} indicate the charging efficiency of a battery, the rate of its self-discharge and efficiency of the converter, respectively. In addition, $P_L(t)$ represents a site's electric load, which can be written as follows:

$$P_L(t) = \begin{cases} P_E(t) & \textit{for HPF configurations} \\ P_E(t) + \frac{P_M(t)}{\eta_{BEF}} & \textit{for BEF configurations} \end{cases} \quad (16)$$

Here, η_{BEF} denotes the BEF efficiency. For maintenance purposes, the battery bank charged capacity should be maintained within safe limits [23]:

$$C_{Batt} \leq C_B(t) \leq (1 - DOD)C_{Batt} \quad (17)$$

Here, C_{Batt} and DOD represent the nominal capacity of the battery and the maximum depth of discharge. DOD is usually considered to be 80% [21].

b. Hydrogen storage:

As an alternative to a battery, hydrogen storage with a lower rate of self-discharge and higher energy density is incorporated in the proposed renewable systems. During a high wind period, hydrogen is generated via electrolysis and stored in hydrogen tanks (HTank). On the other hand, during a low wind period, hydrogen is used to supply electric power through a fuel cell or as fuel for a hydrogen-powered fleet. One can determine the mass of generated hydrogen by via electrolysis using the following equation [24]:

$$M_{H_2,gen}(t) = \eta_{elec} \frac{(P_{w,ac}(t) - P_L(t))\eta_{conv}}{HV_{H_2}/\rho_{H_2}} \quad (18)$$

Here, HV_{H_2}, η_{elec}, and ρ_{H_2} represent the heating value of hydrogen, the efficiency of an electrolyzer and the hydrogen density, respectively. An electrolyzer is assumed to be able to operate above its nominal power (up to double the nominal size) for a limited time. The efficiency/voltage-current chart is used to determine the effect of operating conditions on the electrolyzer efficiency [25]. A hydrogen tank (HTank) is used to store the generated hydrogen. During a low wind period, on the other hand, consuming the stored hydrogen, a fuel cell takes over the electric power supply. The supplied power by the fuel cell can be calculated by:

$$P_{FC}(t) = M_{H_2,cons}(t)\eta_{FC} \frac{HV_{H_2}}{\eta_{conv} \cdot \rho_{H_2}} \quad (19)$$

In this equation, η_{FC} represents the fuel cell efficiency. One can determine the level of the hydrogen tank in the course of charging and discharge by the following equations, respectively:

$$Charging: \quad SH_T(t) = SH_T(t-1) + M_{H_2,gen}(t) \quad (20)$$

$$Discharge: \quad SH_T(t) = SH_T(t-1) - M_{H_2,cons}(t) \quad (21)$$

Note that a fuel cell heat recovery system is incorporated in the proposed configurations for the provision of a site's thermal energy. One can obtain the recovered thermal energy by:

$$P_{hr}(t) = f_{hr} M_{H_2,cons}(t)(1 - \eta_{FC}) \frac{HV_{H_2}}{\eta_{conv} \cdot \rho_{H_2}} \quad (22)$$

Here, f_{hr} denotes the heat recovery ratio.

c. Thermal storage:

The thermal storage is utilized to store the surplus energy during generation and supply the heating demand of the site during wintertime. Incorporating thermal storage into the renewable system design can add significant values to the project and makes more economic sense in terms of storing excess power as opposed to battery storage that could be highly expensive to acquire. A rock-pile thermal storage, due to its comparatively cheaper technology, high capacity, and high thermal efficiency was selected as a thermal storage

unit for the proposed configurations. One can determine the thermal storage level in the course of charging and discharge by:

$$Charging: \quad C_{TS}(t) = C_{TS}(t-1)\eta_{TS} + (P_{w,ac}(t) - P_L(t))\eta_{EB} \tag{23}$$

$$Discharge: \quad C_{TS}(t) = C_{TS}(t-1)\eta_{TS} - P_H(t) \tag{24}$$

Here, η_{EB} and η_{TS} represent the efficiencies of an electric boiler and the thermal storage, respectively.

2.2.3. Mine Mobile Fleet

Fleet electrification is an essential step towards the decarbonization of mine sites. This study offers two different solutions for conventional diesel-powered fleet replacement, namely, a hydrogen-powered fleet, and a battery electric fleet.

a. Battery electric fleet:

Battery electric vehicles are increasingly available and the opportunity for mine fleet electrification has never been better. Electric vehicles have a higher energy efficiency and can be substantially less costly to maintain and operate compared to their diesel counterparts; however, the main challenge for most mining applications of battery electric vehicles is their heavy battery weights and long charging times, which result in a short utilization time. This study offers a battery swapping solution for the mitigation of this issue. Employing vehicles with small size batteries is considered with three charging stations within a hauling route. The batteries would be charged and ready to be picked up by hauling vehicles at these stations. A 5% downtime is assumed for battery swapping at each station. One can determine the BEF electrical demand by:

$$P_{BEF}(t) = \frac{P_M(t)}{\eta_{BEF}} \tag{25}$$

b. Hydrogen-powered fleet:

Employing hydrogen energy for mobile equipment is a growing interest in the mining industry and the utilization of hydrogen can also be a possible option in the decarbonization of mining operations. This technology is evolving, and the manufacturers are bringing new data every day. Unlike their battery electric counterparts, hydrogen-powered vehicles have a shorter refueling period and a lower fuel density. One can calculate the HPF hydrogen demand by:

$$M_{H_2,HPF}(t) = \frac{P_M(t)}{\eta_{HPF} \cdot HV_{H_2}/\rho_{H_2}} \tag{26}$$

2.3. Economic Model

The financial study presented here includes the capital and replacement cost of a fleet, generation power items, storage units, energy conversion and recovery units, operational expenditure, carbon emission penalties, and the earned revenues throughout a mine's lifetime. One can calculate the net present cost (NPC) of each system and the corresponding levelized cost of energy (LCOE) by:

$$\text{NPC} = \sum_{y=0}^{N} \frac{R_y}{(1+i)^y} \tag{27}$$

$$\text{LCOE} = \frac{\text{NPC} \times \text{CRF}}{\sum_{t=0}^{N \times 8760} (P_E(t) + P_M(t) + P_H(t))\Delta t} \tag{28}$$

Here, R_y denotes the year y net cash flow and N represents the lifetime of a project in years. Additionally, i and CRF indicate the rate of the annual real discount and capital recovery factor, which can be determined as follows:

$$i = \frac{i' - f}{1 + f} \tag{29}$$

$$\text{CRF} = \frac{i(1+i)^N}{(1+i)^N - 1} \tag{30}$$

In Equation (29), i' and f represent the rates of nominal discount and inflation, respectively.

The proposed configurations for an alternative mine power plant are wind source renewable energy systems.

3. Results and Discussion

All the conventional diesel-based and the all-renewable alternatives were simulated and optimized via the HOMER Pro Microgrid Software coupled with a user-developed analysis tool. The parameters considered for the simulations and optimizations are given in Table 2. An allocation of 35% of CAPEX is incorporated for the site installation and delivery logistics in remote locations. Note that all the prices considered for economic assessment of the mine energy system are in US dollars.

Table 2. Parameters used for the simulations.

Parameters	Value	Ref	Parameters	Value	Ref
Rate of nominal discount (i')	8%	[26]	The mine lifetime (years)	10	-
Rate of inflation (f)	2%	[26]	Efficiency of fuel cell	0.5	[27]
Capital cost of fuel cell (USD/kW) *	1344	[28]	Efficiency of electrolyzer	0.75	[29,30]
Replacement cost of fuel cell (USD/kW) *	1070	[28]	Efficiency of convertor Battery lifetime (years)	0.95 10	[21] [30]
Capital cost of battery (USD/kWh) *	350	[30]	Fuel cell lifetime (years)	5	[27]
Replacement cost of battery (USD/kWh) *	300	[30]	Diesel truck lifetime (years)	2	[28]
Capital cost of diesel truck (USD/kW)	1139	[28]	Hydrogen-powered truck lifetime (years) Battery electric truck lifetime (years)	2 2	[28,31] [28,31]
Replacement cost of diesel truck (USD/kW)	1139	[28]	Electrolyzer lifetime (years)	10	[32]
Capital cost of hydrogen-powered truck (USD/kW)	1709	[28,31]	Turbine lifetime (years)	20	[33]
Replacement cost of hydrogen-powered truck (USD/kW)	1709	[28,31]	Convertor lifetime (years)	15	[21]
Capital cost of battery electric truck (USD/kW)	1709	[28,31]	HTank lifetime (years)	20	[27]
Replacement cost of battery electric truck (USD/kW)	1709	[28,31]	Price of diesel (USD/L) Capital cost of diesel generator (USD/kW)	0.81 900	[34] [35]
Capital cost of electrolyzer (USD/kW) *	1100	[30,36]	Replacement cost of diesel generator (USD/kW)	900	[35]

Table 2. *Cont.*

Parameters	Value	Ref	Parameters	Value	Ref
Replacement cost of electrolyzer (USD/kW) *	825	[30,36]	Capital cost of thermal storage (USD/MWh)	544.72	[15]
Capital cost of HTank (USD/kg)	574.22	[37]	Carbon emission penalty (USD/tonne)	35	[17]
Replacement cost of HTank (USD/kg)	574.22	[37]	Convertor capital cost (USD/kw)	300	[21]
Capital cost of wind turbine (USD/kW)	1970	[38]	Replacement cost of convertor (USD/kW)	300	[21]
Replacement cost of wind turbine (USD/kW)	1970	[38]	Swapping batteries lifetime	1	[28]
Lower heating value of diesel (MJ/kg)	43.2	[39]	Fuel cell heat recovery ratio	60	[39]
Density of diesel (kg/m^3)	820	[39]	Thermal storage efficiency	90	[15]
Density of H_2 (kg/m^3) (MJ/kg)	0.09	[39]	Electric boiler efficiency	95	[40]
Lower heating value of H_2 (MJ/kg)	120	[39]	Battery bank roundtrip efficiency	90	[39]

* Excluding costs of installation and delivery logistics.

3.1. Case Study

To achieve a practical appreciation of the concept, an off-grid location in Nunavut was considered as a case study. The ambient air temperature and local wind speed were acquired for the site from the Canadian Weather and NASA Surface Meteorology and Solar Energy databases, respectively. Figure 9 shows the site's monthly averaged wind speed data. As it can be inferred from this figure, the studied location with the annual average wind speed of 6.5 m/s has a great potential for wind energy harvesting. In addition, using the ambient air temperature data, the site's modular size scale heating demand for two different mining cases of surface mines with minimal and intensive C&MP were calculated, with the results illustrated in Figure 10.

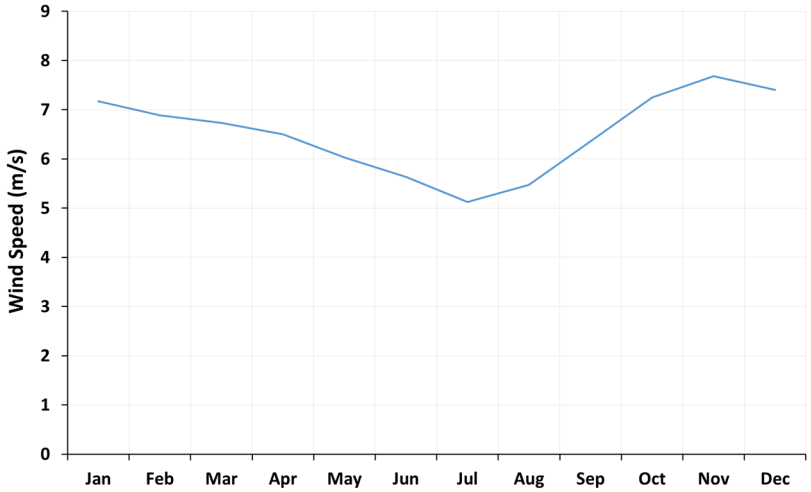

Figure 9. The site's monthly averaged wind speed data [41].

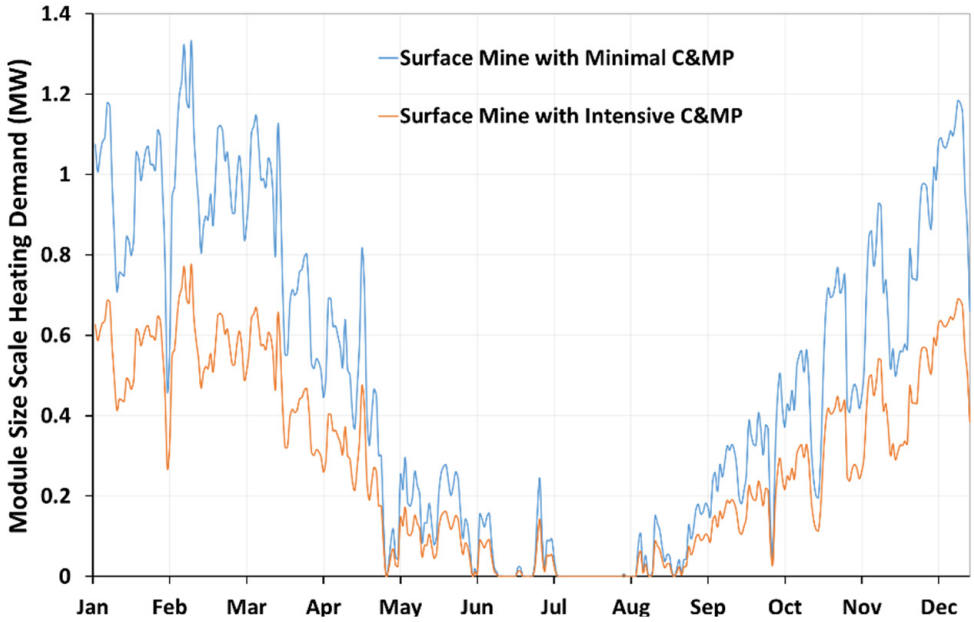

Figure 10. The site's modular size scale heating demands for minimal and intensive C&MP scenarios.

3.2. Main Installations and Corresponding Costs

According to the results of the simulations and optimizations conducted in HOMER Pro, coupled with a user-developed analysis tool for each mining scenario, the site will require key equipment installations. Tables 3 and 4 summarize the main equipment installations required at the site for each case and their corresponding levelized cost of energy based on the results generated by the optimization process. According to the results of the evaluation, replacing the mine's diesel-based power plant with an all-renewable energy system not only reduces the carbon footprint of the operation substantially, but also with a proper design it can give better economic returns when comparing it to a conventional diesel-based system. As it can be noted from these tables, for the surface mine with intensive C&MP, employing renewable energy systems makes more financial sense as their levelized cost of energy is lower compared to the minimal C&MP scenario. This cost difference can be traced back to the higher proportion of motive power demand for the mine with a minimal C&MP compared to its intensive counterpart (see Figure 1). The decarbonization of motive power is more costly than heating and electric power. For the motive power, in addition to the costs of a power generation unit (for vehicle fuel supply), the electrification of a fleet imposes an extra financial burden on the project. Moreover, as it can be seen from these tables, for both types of surface mining operations (i.e., minimal and intensive C&MP), a renewable design with a Battery/FC storage and hydrogen-powered fleet configuration returns the most profitable case. Two points can be noted here: firstly, for surface mining operations, hydrogen-powered vehicles are less costly than battery electric vehicles which is due to the longer downtime of a BEF, and secondly, hybridizing a battery and fuel cell to meet the power shortage would add considerable financial value to the proposed decarbonization project.

Table 3. Installation capacities and economic–environmental results for minimal C&MP scenario in 5 MW modular size scale.

Installation	Scenario: Minimal C&MP						
	DPF	HPF			BEF		
		Batt. and FC	FC	Batt.	Batt. and FC	FC	Batt.
Diesel generator (MW)	4.5	-			-	-	-
Diesel boiler (kW)	1400	-			-	-	-
Wind turbine (MW)	-	31.5	33	30	28.5	31.5	31.5
Battery (MWh)	-	11	-	31	19	-	146
Converter (MW)	-	26	30	25	19	19	19
Fuel cell (MW)	-	1.2	3	-	5.5	7	-
Electrolyzer (MW)	-	26	27	24	15	14	-
H_2 tank (tonne)	-	23	24	24	11	14	-
Thermal storage (MWh)	-	130	80	90	80	70	50
Electric heater (kW)	-	2000	3100	3400	1300	1200	1100
Mobile fleet (kW)	2700	2700	2700	2700	4800	4800	4800
CO_2 emissions (tonne/yr)	26,000	-	-	-	-	-	-
LCOE (USD/kWh)	0.47	0.47	0.48	0.48	0.66	0.68	0.77

Table 4. Installation capacities and economic–environmental results for intensive C&MP scenario in 5MW modular size scale.

Installation	Scenario: Intensive C&MP						
	DPF	HPF			BEF		
		Batt. and FC	FC	Batt.	Batt. and FC	FC	Batt.
Diesel generator (MW)	7	-			-	-	-
Diesel boiler (kW)	800	-			-	-	-
Wind turbine (MW)	-	27	30	25.5	28.5	31.5	27
Battery (MWh)	-	22	-	64	10	-	157
Converter (MW)	-	21	19	15	18	14	17
Fuel cell (MW)	-	1.8	5	-	6	7	-
Electrolyzer (MW)	-	20	20	15	12.5	12	-
H_2 tank (tonne)	-	20	25	20	11	13	-
Thermal storage (MWh)	-	60	50	60	50	40	30
Electric heater (kW)	-	1000	750	1100	700	650	700
Mobile fleet (kW)	1600	1600	1600	1600	2800	2800	2800
CO_2 emissions (tonne/yr)	28,000	-	-	-	-	-	-
LCOE (USD/kWh)	0.47	0.41	0.43	0.44	0.51	0.53	0.62

3.3. Parametric Analysis

To provide a wider spectrum of the economic viability of employing the proposed all-renewable system for surface mining operations in different locations, at the present time and in a future perspective, wind speed/renewable market price sensitivity analyses were conducted. As mentioned before, among the storage configurations, hybridized battery and hydrogen storage returns the most profitable case; therefore, it was selected for the parametric study. Figure 11 shows the impact of wind speed variation on the economics of the system with the current renewable market. The red line represents a conventional all-diesel based system (Figure 2). The green line indicates an all-renewable system with a hydrogen-powered fleet and battery and fuel cell storage configuration (Figure 3). The blue line corresponds to an all-renewable system with a battery electric fleet and battery and fuel cell storage configuration (Figure 6). As the figure shows, when it comes to the fleet configuration, hydrogen-powered trucks are better candidates as a solution for both types of surface mining operations, at all the studied wind speeds. In addition, as it can be inferred from the figure, with the current renewable market prices, for the implementation of an all-renewable system at a mine site, an annual average wind speed of at least 6.5 m/s

for surface mines with minimal C&MP, and 6 m/s for surface mines with intensive C&MP is required.

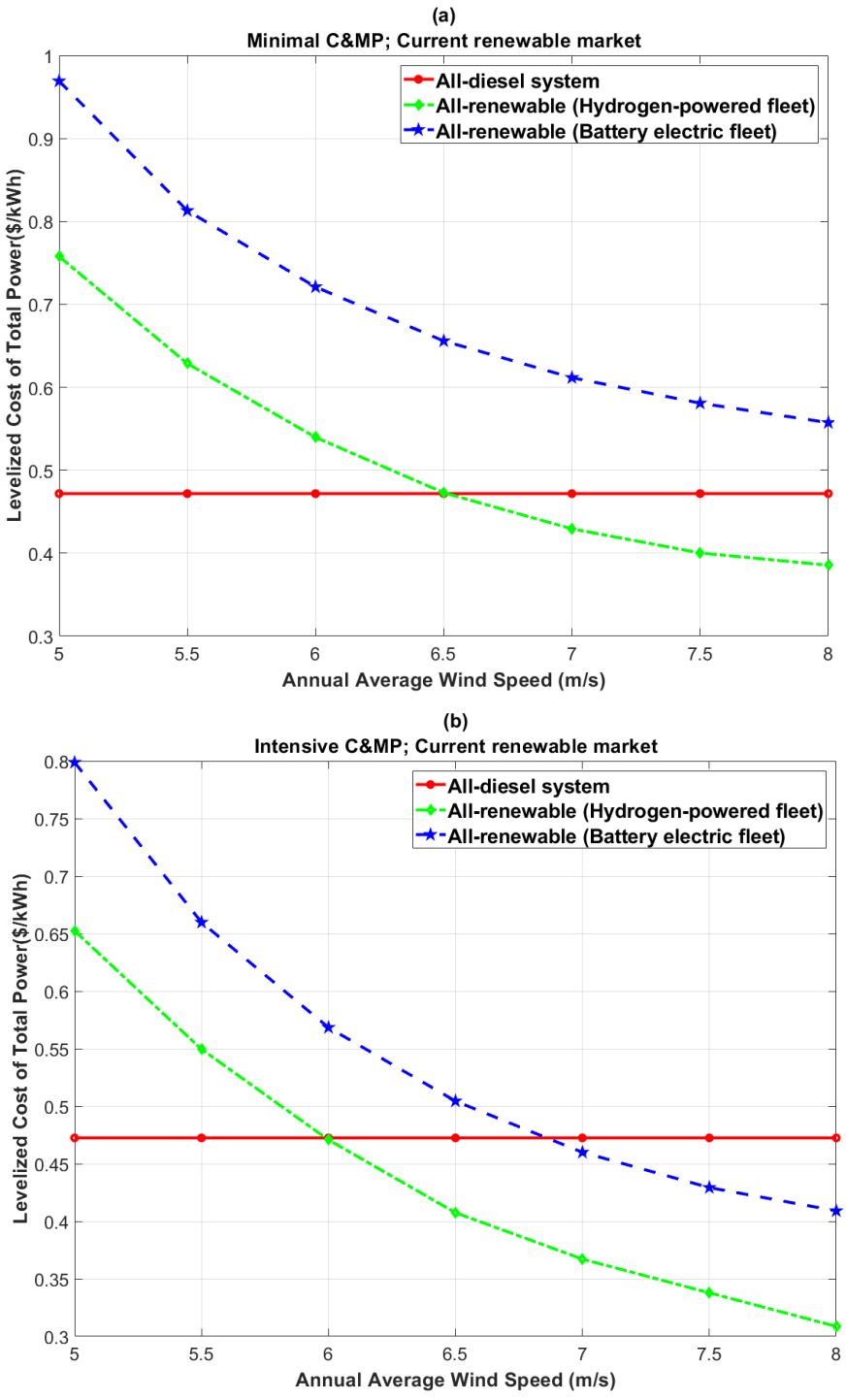

Figure 11. Wind speed impact on all-renewable system (Battery and FC storage config.) with the current renewable market: (**a**) surface mine with minimal C&MP; (**b**) surface mine with intensive C&MP.

The results of the sensitivity analysis show that for mine sites with annual wind speeds of less than 6 m/s, employing a fully decarbonized renewable system may not be very economically feasible with the current market prices. Renewables have high market prices today, which are the main restrictive factors in fully transitioning a mine energy system off diesel; however, according to the International Renewable Energy Agency, onsite renewable energy generation (i.e., wind farms and solar panels) will be effectively cheaper

than diesel power in the near future [42]. To this end, in this study, the future prospect of renewables implementation for mine sites were evaluated by assuming a 20% and 40% drop in renewable technology implementation costs (i.e., wind turbines, batteries, fuel cells, electrolyzers and the electrification costs of a fleet). Figures 12 and 13 depict the results of this evaluation. As can be seen from these figures, with a 20% decrease in renewable technology prices, the proposed all-renewable energy system could be installed for sites with annual average wind speeds of less than 6 m/s. This figure is reduced to less than 5.5 m/s with a 40% drop in the renewables market.

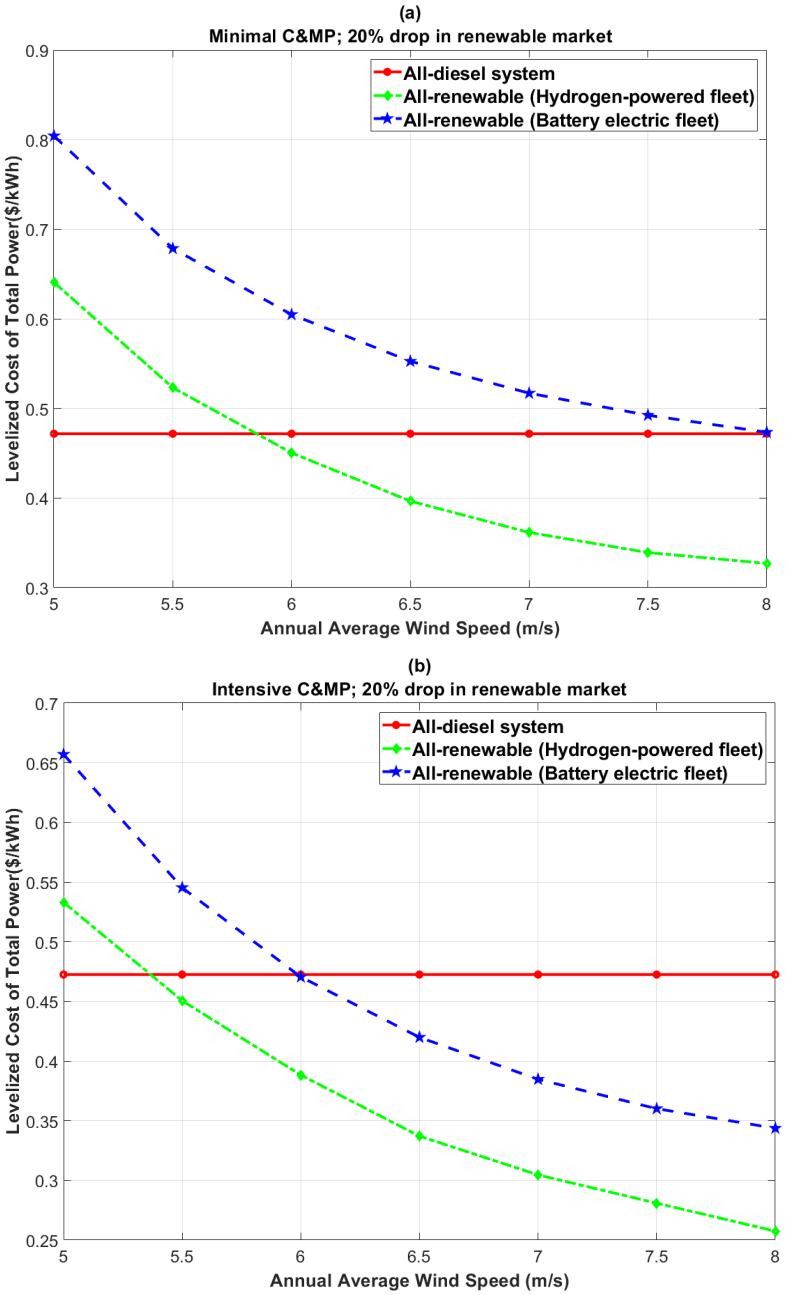

Figure 12. Wind speed impact on all-renewable system (Battery and FC storage config.) with 20% drop in renewable market: (**a**) surface mine with minimal C&MP; (**b**) surface mine with intensive C&MP.

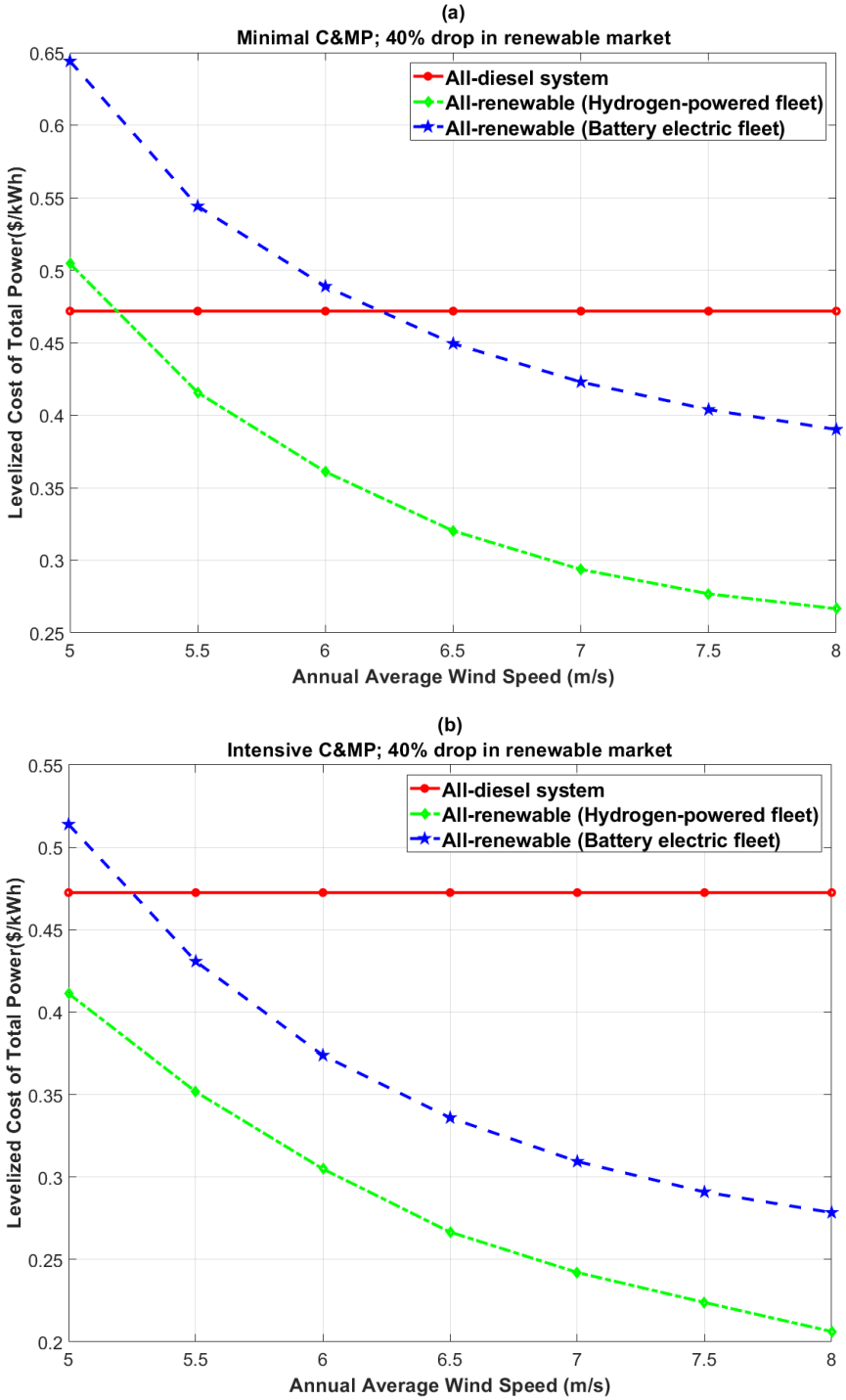

Figure 13. Wind speed impact on all-renewable system (Battery and FC storage config.) with 40% drop in renewable market: (**a**) surface mine with minimal C&MP; (**b**) surface mine with intensive C&MP.

The sensitivity evaluation conducted in this study was with the wind speed pattern for the case study location. The wind speed pattern has a significant effect on the economics of the proposed all-renewable energy system, especially the sizing of the storage units (i.e., battery, hydrogen and thermal storages). Figure 14 shows the wind speed pattern effect on renewable power generation and the hydrogen tank level. As it can be inferred from this figure, during a low-wind period, as the generation part of the fully decarbonized system fails to satisfy a site's total energy needs, the storage units should be large enough to supply

the site's total power demands; therefore, the longer the low-wind period is, the higher that storage units are required for the system which drives the costs up to prohibitive levels.

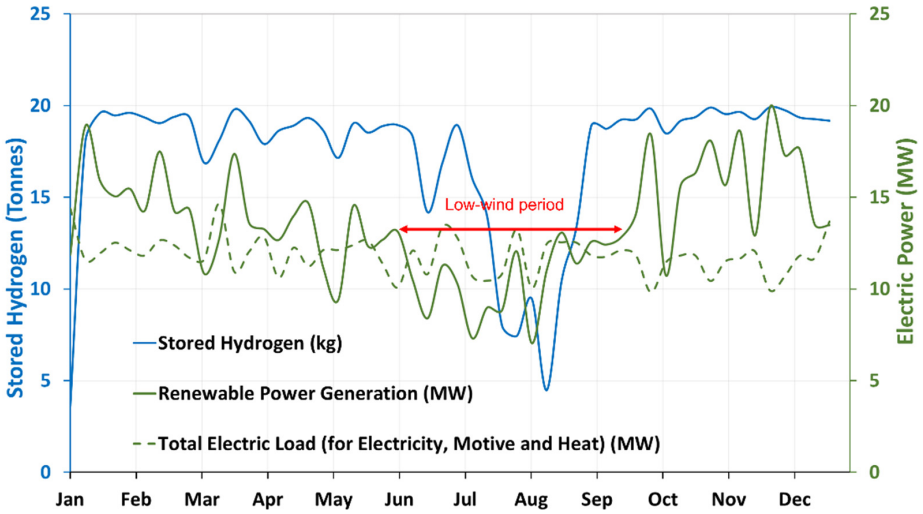

Figure 14. Low-wind period effect on renewable power generation and hydrogen storage level 4.

4. Conclusions

The feasibility of employing a stand-alone fully decarbonized renewable system with a novel integration of multi-storage units (e.g., battery–hydrogen–rock pile thermal storage) for arctic remote surface mines was investigated. Six different configurations for all-renewable systems were proposed and the results were compared with the conventional all-diesel based system. It has been found that, for open-pit mining operations (both intensive and minimal C&MP), renewable systems with a hydrogen-powered fleet and hybridized battery/hydrogen storage configuration yields better performances in all technical, environmental, and economic aspects. It was shown that the system with a HPF configuration results in substantial carbon emission reductions at the net present costs, which are competitive (if not lower than) with conventional diesel-based systems. The simulation results indicated that for a viable operation of any fully decarbonized renewable system implemented in arctic remote mine sites and operating under current renewable energy market prices, a minimum annual average wind speed of 6 m/s is required; however, as the renewable solutions are becoming consistently less expensive, even mine sites with comparatively medium/low wind speeds can benefit from renewable energy implementations in the near future. Most importantly, the results of this study highlighted the significant impact of a low-wind period on the storage size and techno-economic feasibility of a fully decarbonized mine energy system. Under this analogy, sites experiencing longer low-wind periods require storage units with higher capacities which can be a cost- prohibitive factor.

Author Contributions: Conceptualization, H.K. and S.A.G.-M.; methodology, H.K. and S.A.G.-M.; software, H.K.; validation, H.K.; formal analysis, H.K. and S.A.G.-M.; investigation, H.K. and S.A.G.-M.; resources, H.K. and S.A.G.-M.; data curation, H.K. and S.A.G.-M.; writing—original draft preparation, H.K.; writing—review and editing, H.K. and S.A.G.-M.; visualization, H.K. and S.A.G.-M.; supervision, S.A.G.-M.; project administration, S.A.G.-M.; funding acquisition, S.A.G.-M. All authors have read and agreed to the published version of the manuscript.

Funding: This research received no external funding.

Institutional Review Board Statement: Not applicable.

Informed Consent Statement: Not applicable.

Data Availability Statement: Not applicable.

Conflicts of Interest: The authors declare no conflict of interest.

References

1. Bharathan, B.; Sasmito, A.P.; Madiseh, S.A.G. Analysis of energy consumption and carbon footprint from underground haulage with different power sources in typical Canadian mines. *J. Clean. Prod.* **2017**, *166*, 21–31. [CrossRef]
2. Climate Risk and Decarbonization: What Every Mining CEO Needs to Know | McKinsey. Available online: https://www.mckinsey.com/business-functions/sustainability/our-insights/climate-risk-and-decarbonization-what-every-mining-ceo-needs-to-know (accessed on 3 June 2022).
3. Diavik Diamond Mine Made a Wind Farm for Power | Mining & Energy. Available online: https://www.miningandenergy.ca/sustainability/article/diavik_diamond_mine_turns_to_wind/ (accessed on 17 August 2021).
4. Glencore RAGLAN Mine Renewable Electricity Smart-Grid Pilot Demonstration. Available online: https://www.nrcan.gc.ca/science-and-data/funding-partnerships/funding-opportunities/current-investments/glencore-raglan-mine-renewable-electricity-smart-grid-pilot-demonstration/16662 (accessed on 17 August 2021).
5. Rieussec, E. Greenhouse Gas Emissions Canadian Environmental Sustainability Indicators. Available online: https://www.canada.ca/content/dam/eccc/documents/pdf/cesindicators/ghg-emissions/2022/ghg-emissions-en.pdf/ (accessed on 11 June 2022).
6. Hlal, M.I.; Ramachandaramurthy, V.K.; Sarhan, A.; Pouryekta, A.; Subramaniam, U. Optimum battery depth of discharge for off-grid solar PV/battery system. *J. Energy Storage* **2019**, *26*, 100999. [CrossRef]
7. Journal, T.; Salkuti, S.R. Comparative analysis of electrochemical energy storage technologies for smart grid. *TELKOMNIKA Telecommun. Comput. Electron. Control.* **2020**, *18*, 2118–2124. [CrossRef]
8. Uyar, T.S.; Beşikci, D. Integration of hydrogen energy systems into renewable energy systems for better design of 100% renewable energy communities. *Int. J. Hydrogen Energy* **2017**, *42*, 2453–2456. [CrossRef]
9. Calderón, M.; Calderón, A.J.; Ramiro, A.; González, J.F.; González, I. Evaluation of a hybrid photovoltaic-wind system with hydrogen storage performance using exergy analysis. *Int. J. Hydrogen Energy* **2011**, *36*, 5751–5762. [CrossRef]
10. Kalinci, Y.; Dincer, I.; Hepbasli, A. Energy and exergy analyses of a hybrid hydrogen energy system: A case study for Bozcaada. *Int. J. Hydrogen Energy* **2017**, *42*, 2492–2503. [CrossRef]
11. Marchenko, O.V.; Solomin, S.V. Modeling of hydrogen and electrical energy storages in wind/PV energy system on the Lake Baikal coast. *Int. J. Hydrogen Energy* **2017**, *42*, 9361–9370. [CrossRef]
12. Dursun, B. Determination of the optimum hybrid renewable power generating systems for Kavakli campus of Kirklareli University, Turkey. *Renew. Sustain. Energy Rev.* **2012**, *16*, 6183–6190. [CrossRef]
13. Khalid, F.; Dincer, I.; Rosen, M.A. Analysis and assessment of an integrated hydrogen energy system. *Int. J. Hydrogen Energy* **2016**, *41*, 7960–7967. [CrossRef]
14. Lundh, M.; Dalenbäck, J.O. Swedish solar heated residential area with seasonal storage in rock: Initial evaluation. *Renew. Energy* **2008**, *33*, 703–711. [CrossRef]
15. Amiri, L.; De Brito, M.A.R.; Baidya, D.; Kuyuk, A.F.; Ghoreishi-Madiseh, S.A.; Sasmito, A.P.; Hassani, F.P. Numerical investigation of rock-pile based waste heat storage for remote communities in cold climates. *Appl. Energy* **2019**, *252*, 113475. [CrossRef]
16. Kalantari, H.; Ghoreishi-Madiseh, S.A.; Sasmito, A.P. Hybrid Renewable Hydrogen Energy Solution for Application in Remote Mines. *Energies* **2020**, *13*, 6365. [CrossRef]
17. Benchmarking Guides. Available online: https://www.nrcan.gc.ca/energy-efficiency/energy-efficiency-industry/energy-management-industry/energy-benchmarking-industry/benchmarking-guides/5171#ll (accessed on 17 August 2021).
18. HOMER—Hybrid Renewable and Distributed Generation System Design Software. Available online: https://www.homerenergy.com/ (accessed on 17 August 2021).
19. Mora, M.A.M.; Vergara, F.C.P.; Delgadillo, S.A.M.; Leiva, M.A. Comparison of carbon balance measuring tools in an enhanced oil recovery project based on the carbon dioxide from the ammonia production process streams. *J. Clean. Prod.* **2017**, *144*, 540–552. [CrossRef]
20. Genç, M.S.; Çelik, M.; Karasu, I. A review on wind energy and wind–hydrogen production in Turkey: A case study of hydrogen production via electrolysis system supplied by wind energy conversion system in Central Anatolian Turkey. *Renew. Sustain. Energy Rev.* **2012**, *16*, 6631–6646. [CrossRef]
21. Al-Sharafi, A.; Sahin, A.Z.; Ayar, T.; Yilbas, B.S. Techno-economic analysis and optimization of solar and wind energy systems for power generation and hydrogen production in Saudi Arabia. *Renew. Sustain. Energy Rev.* **2017**, *69*, 33–49. [CrossRef]
22. Diaf, S.; Diaf, D.; Belhamel, M.; Haddadi, M.; Louche, A. A methodology for optimal sizing of autonomous hybrid PV/wind system. *Energy Policy* **2007**, *35*, 5708–5718. [CrossRef]
23. Anoune, K.; Bouya, M.; Astito, A.; Ben Abdellah, A. Sizing methods and optimization techniques for PV-wind based hybrid renewable energy system: A review. *Renew. Sustain. Energy Rev.* **2018**, *93*, 652–673. [CrossRef]
24. Hakimi, S.M.; Moghaddas-Tafreshi, S.M. Optimal sizing of a stand-alone hybrid power system via particle swarm optimization for Kahnouj area in south-east of Iran. *Renew. Energy* **2009**, *34*, 1855–1862. [CrossRef]
25. Flamm, B.; Peter, C.; Büchi, F.N.; Lygeros, J. Electrolyzer modeling and real-time control for optimized production of hydrogen gas. *Appl. Energy* **2021**, *281*, 116031. [CrossRef]
26. Hydrogen and Fuel Cell Technologies Office Multi-Year Research, Development, and Demonstration Plan | Department of Energy. Available online: https://www.energy.gov/eere/fuelcells/downloads/hydrogen-and-fuel-cell-technologies-office-multi-year-research-development (accessed on 17 August 2021).

27. Fathy, A. A reliable methodology based on mine blast optimization algorithm for optimal sizing of hybrid PV-wind-FC system for remote area in Egypt. *Renew. Energy* **2016**, *95*, 367–380. [CrossRef]
28. Caterpillar 797. Available online: https://www.caranddriver.com/reviews/a15140071/caterpillar-797-specialty-file/ (accessed on 17 August 2021).
29. Harrison, K.; Peters, M. Renewable Electrolysis Integrated System Development & Testing. In Proceedings of the 2014 DOE Hydrogen and Fuel Cells Program Review, Washington, DC, USA, 16–20 June 2014.
30. Krishan, O.; Suhag, S. Techno-economic analysis of a hybrid renewable energy system for an energy poor rural community. *J. Energy Storage* **2019**, *23*, 305–319. [CrossRef]
31. Varaschin, J.; De Souza, E. Economics of diesel fleet replacement by electric mining equipment. In Proceedings of the 15th North American Mine Ventilation Symposium, Blacksburg, VA, USA, 20–25 June 2015.
32. Esposito, D.V. Membraneless Electrolyzers for Low-Cost Hydrogen Production in a Renewable Energy Future. *Joule* **2017**, *1*, 651–658. [CrossRef]
33. Gabbar, H.A.; Abdussami, M.R.; Adham, M.I. Techno-Economic Evaluation of Interconnected Nuclear-Renewable Micro Hybrid Energy Systems with Combined Heat and Power. *Energies* **2020**, *13*, 1642. [CrossRef]
34. Transportation Fuel Prices. Available online: https://www.nrcan.gc.ca/our-natural-resources/domestic-and-international-markets/transportation-fuel-prices/4593 (accessed on 17 August 2021).
35. Garcia, R.S.; Weisser, D. A wind–diesel system with hydrogen storage: Joint optimisation of design and dispatch. *Renew. Energy* **2006**, *31*, 2296–2320. [CrossRef]
36. Chi, J.; Yu, H. Water electrolysis based on renewable energy for hydrogen production. *Chin. J. Catal.* **2018**, *39*, 390–394. [CrossRef]
37. Luta, D.N.; Raji, A.K. Optimal sizing of hybrid fuel cell-supercapacitor storage system for off-grid renewable applications. *Energy* **2019**, *166*, 530–540. [CrossRef]
38. Ahmad, J.; Imran, M.; Khalid, A.; Iqbal, W.; Ashraf, S.R.; Adnan, M.; Ali, S.F.; Khokhar, K.S. Techno economic analysis of a wind-photovoltaic-biomass hybrid renewable energy system for rural electrification: A case study of Kallar Kahar. *Energy* **2018**, *148*, 208–234. [CrossRef]
39. Finding Data to Run HOMER. Available online: https://www.homerenergy.com/products/pro/docs/latest/finding_data_to_run_homer.html (accessed on 17 August 2021).
40. Khojasteh-Salkuyeh, Y.; Ashrafi, O.; Mostafavi, E.; Navarri, P. CO_2 utilization for methanol production; Part I: Process design and life cycle GHG assessment of different pathways. *J. CO_2 Util.* **2021**, *50*, 101608. [CrossRef]
41. NASA. Power Data Access View. 2019. Available online: https://power.larc.nasa.gov/data-access-viewer/ (accessed on 17 August 2019).
42. CIM Magazine February 2022 by CIM-ICM Publications—Issuu. Available online: https://issuu.com/cim-icm_publications/docs/february2022_full (accessed on 3 June 2022).